Computer simulation of apolar bent-core and rodlike molecules

Stephen J. Johnston, Robert J. Low, and Maureen P. Neal*
School of Mathematical and Information Sciences, Coventry University, Coventry, CV1 5FB, United Kingdom
(Received 31 October 2001; published 2 May 2002)

Bent-core molecules have received much interest due to their biaxiality and novel phase ordering. It is, therefore, of interest to model the characteristic shape of these molecules and observe the effect on liquid crystal mesophase formation in a computer simulation study. A simple model of the interaction employed a two-site Gay-Berne potential with the sites separated by ± 0.5 reduced units for all models. The angle between the two sites, $180° - \gamma$, was varied from $\gamma = 0°$ to $\gamma = 70°$ and influenced the phase behavior markedly. The rodlike model formed isotropic, nematic, smectic-*A*, and smectic-*B*, phases. Results for the bent-core models show that as the angle γ increases the transition temperature to the ordered phase decreases. As γ increases the nematic phase is first destabilized then stabilized with respect to the smectic phase and a tilted smectic-*B* phase is seen at $\gamma = 20°$. For $\gamma = 40°$ a ''TGB-like'' phase is identified as the system cools whereas for $\gamma = 70°$ no ordered phase is formed.

DOI: 10.1103/PhysRevE.65.051706 PACS number(s): 61.20.Ja

I. INTRODUCTION

The first report of bent-core liquid crystalline systems was made by Niori *et al.* [1] in 1996. They received immediate interest due to their ferroelectric properties [1] and later due to their ability to form chiral phases, as described in Ref. [2], despite the constituent molecules being achiral. Polar alignment of molecules constrained to a smectic layer is the structure proposed in this first paper [1] to explain the ferroelectric ordering. Much research, see, e.g., Refs. [3–7] has been conducted after this seminal paper. The majority report on the transition from the isotropic phase directly to smecticlike phases, an exception [3] being a transition to an intermediate nematic phase before the smectic. All studies report on either ferroelectric, e.g., Refs. [4,5] or antiferroelectric [6,7] alignment. The great majority report on chiral structures in the mesophases formed. Most liquid crystals are incapable of forming ferroelectric phases due to the high degree of symmetry, typically $D_{\infty h}$, in the system preventing macroscopic polarization [8]. It is believed that efficient steric packing causes a layered structure to develop reducing the symmetry to a C_{2v} group [1]. This allows for alignment of the molecular transverse dipoles along the C_2 axis and for ferroelectric or antiferroelectric order to develop depending on the alignment of the dipoles. This is the structure reported by [1]. Later studies, e.g., Refs. [6,9] describe a structure where the molecules are tilted with respect to the layer normal. This reduces the symmetry further to a C_2 group, which leads to chiral phases. Left and right handed helices are distinguished by the direction of tilt of the molecules within the layer. The angle between the wings of the molecule has been reported to vary between 100° and 135° [7,10–12].

Computer simulation provides the opportunity to study the generalized shape of a group of molecules and assess the impact of shape on the phase behavior of the system [13]. Previous studies have used a variety of potentials ranging from realistic simulations, e.g., Refs. [14–16], which provide data comparable to experiment but are computationally expensive, to hard anisotropic models [17,18] that are based purely on steric shape and include no attractive forces but which are nonetheless successful in reproducing some liquid crystal phases.

An anisotropic potential such as the Gay-Berne potential [19] has terms that describe the repulsive core of the molecule as well as including attractive forces. Such a potential has the advantage of being computationally inexpensive compared with the realistic potentials currently in use. The behavior of molecular models simulated using single site Gay-Berne potentials has been extensively studied, e.g., Refs. [20–23]. The rich diversity of phases that the Gay-Berne potential has reproduced in simulation studies has contributed to its popularity. The liquid crystal phases observed include the nematic, smectic-*A*, and smectic-*B* phases. Additional interaction potentials used in conjunction with the Gay-Berne potential have displayed chiral [24] and tilted phases [25]. The Gay-Berne potential is, therefore, adaptable and highly useful in the study of liquid crystal behavior.

Previous simulation studies of two-site hard spherocylinders and soft Gay-Berne models have failed to show any of the novel packing structures seen in real bent-core molecules. Hard rod simulation studies have produced classical liquid crystal phases [26] and a soft anisotropic model [27] showed some evidence of a chiral superstructure although this has yet to be confirmed. A recent report by Xu *et al.* [28] who used a bent-core model composed of seven Lennard-Jones sites details a tilted layered system, the first report of chiral symmetry breaking behavior in an achiral bent-core system due to steric effects alone. Glaser and co-workers [29], who examined a mixture of calamitic and bent-core molecules found short-range synclinic tilts. A Monte Carlo study of a system of hard bent cores [30] with length-to-breadth ratio of 10:1 for the rodlike case found that, for a value of $\gamma = 15°$, there was a transition from a nonpolar to a steric ''polar'' smectic phase, although the model was electrically apolar. For $\gamma > 45°$ the nematic phase was destabilized relative to the smectic phase. The steric and electro-

*Corresponding author. Email address: m.p.neal@coventry.ac.uk

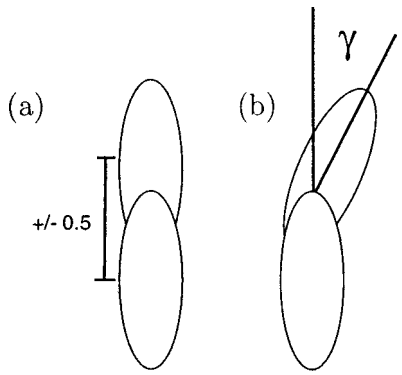

FIG. 1. Schematic representation of the geometry of (a) a two-site cylinder and (b) a two-site bent-core shape.

static factors influence the in-layer tilt and thereby spontaneous symmetry breaking remains of key interest [31–33].

In the molecular dynamics study reported here we employ a two-site Gay-Berne potential to model the effect of varying the angle by which the two subunits are joined as shown in Fig. 1(b). The bent-core models investigated here are for values of $\gamma=0°,10°,20°,40°$, and 70° where for $\gamma=0°$, the rodlike model, the length-to-breadth ratio is 4:1. These values were chosen to give a range of values that would allow determination of the effect of the variation of γ from the rodlike case and also to include the values found in real molecules of $\gamma=45°$ to $\gamma=80°$. A current study examines the effect of the addition of a transverse dipole upon the phase diagram [34].

The paper is organized as follows: in Sec. II, we describe the model and the details of the simulation, the results of the simulation are presented in Sec. III, and conclusions in Sec. IV.

II. SIMULATION AND MODEL

A. Model

To model the characteristic shape of the bent-core mesogens, a two-site Gay-Berne [19] potential was employed. The centers of mass in the model are displaced by ± 0.5 reduced units along the x axis [see Figs. 1(a) and 1(b)] in every case. This gave an overall length of four reduced units and a width of one reduced unit for the rod with $\gamma=0°$, a similar ratio to that of a real bent-core shaped mesogen, e.g., P-*n*-PIMB [1]. The Gay-Berne potential that models the anisotropic interaction between the two molecules *i* and *j*, considered as ellipsoids, is given by

$$U_{GB}(\hat{\mathbf{u}}_i,\hat{\mathbf{u}}_j,\hat{\mathbf{r}}_{ij}) = 4\epsilon(\hat{\mathbf{u}}_i,\hat{\mathbf{u}}_j,\hat{\mathbf{r}}_{ij}) \times\left\{\left(\frac{\sigma_o}{[r_{ij}-\sigma(\hat{\mathbf{u}}_i,\hat{\mathbf{u}}_j,\hat{\mathbf{r}}_{ij})+\sigma_o]}\right)^{12} -\left(\frac{\sigma_o}{[r_{ij}-\sigma(\hat{\mathbf{u}}_i,\hat{\mathbf{u}}_j,\hat{\mathbf{r}}_{ij})+\sigma_o]}\right)^{6}\right\}, \quad (1)$$

where $\hat{\mathbf{u}}_i$ and $\hat{\mathbf{u}}_j$ are the orientational unit vectors and $\mathbf{r}_{ij}$ is the site-site intermolecular vector linking the centers of mass. The strength of the interaction is given by the strength anisotropy function ϵ

$$\epsilon(\hat{\mathbf{u}}_i,\hat{\mathbf{u}}_j,\hat{\mathbf{r}}_{ij}) = \epsilon_o\epsilon_1^{\nu}(\hat{\mathbf{u}}_i,\hat{\mathbf{u}}_j)\epsilon_2^{\mu}(\hat{\mathbf{u}}_i,\hat{\mathbf{u}}_j,\hat{\mathbf{r}}_{ij}), \quad (2)$$

where μ and ν are adjustable exponents and ϵ_o is a constant. ϵ_1 is defined by

$$\epsilon_1(\hat{\mathbf{u}}_i,\hat{\mathbf{u}}_j) = [1-\chi^2(\hat{\mathbf{u}}_i\cdot\hat{\mathbf{u}}_j)^2]^{-1/2} \quad (3)$$

and ϵ_2 by

$$\epsilon_2(\hat{\mathbf{u}}_i,\hat{\mathbf{u}}_j,\hat{\mathbf{r}}_{ij}) = 1-\frac{\chi'^2}{2}\left(\frac{(\hat{\mathbf{r}}_{ij}\cdot\hat{\mathbf{u}}_i+\hat{\mathbf{r}}_{ij}\cdot\hat{\mathbf{u}}_j)^2}{1+\chi'\hat{\mathbf{u}}_i\cdot\hat{\mathbf{u}}_j} + \frac{(\hat{\mathbf{r}}_{ij}\cdot\hat{\mathbf{u}}_i-\hat{\mathbf{r}}_{ij}\cdot\hat{\mathbf{u}}_j)^2}{1-\chi'\hat{\mathbf{u}}_i\cdot\hat{\mathbf{u}}_j}\right). \quad (4)$$

χ' quantifies the anisotropy in the attractive forces and is defined in terms of the well depths ϵ_s in the side-to-side configuration and ϵ_e in the end-to-end configuration.

$$\chi' = \frac{1-(\epsilon_e/\epsilon_s)^{1/\mu}}{1+(\epsilon_e/\epsilon_s)^{1/\mu}}. \quad (5)$$

Information about the shape of the molecule is then contained in the orientation-dependent range parameter,

$$\sigma(\hat{\mathbf{u}}_i,\hat{\mathbf{u}}_j,\hat{\mathbf{r}}_{ij}) = \sigma_o\left[1-\frac{\chi}{2}\left(\frac{(\hat{\mathbf{r}}_{ij}\cdot\hat{\mathbf{u}}_i+\hat{\mathbf{r}}_{ij}\cdot\hat{\mathbf{u}}_j)^2}{1+\chi\hat{\mathbf{u}}_i\cdot\hat{\mathbf{u}}_j} + \frac{(\hat{\mathbf{r}}_{ij}\cdot\hat{\mathbf{u}}_i-\hat{\mathbf{r}}_{ij}\cdot\hat{\mathbf{u}}_j)^2}{1-\chi\hat{\mathbf{u}}_i\cdot\hat{\mathbf{u}}_j}\right)\right]^{-1/2}. \quad (6)$$

The parameter χ is defined by

$$\chi = \frac{(\sigma_e/\sigma_s)^2-1}{(\sigma_e/\sigma_s)^2+1}, \quad (7)$$

where σ_e/σ_s is the ratio of separations when the potential $U=0$, σ_e for the end-to-end configuration and σ_s for the side-to-side configuration. In this case $\sigma_0=\sigma_s$.

Previous studies have extensively studied the phase behavior of the single-site Gay-Berne fluid [20,21,35] for the parameters $\sigma_e/\sigma_s=3$ and $\epsilon_e/\epsilon_s=0.2$ for different sets of exponents, ($\nu=3,\mu=1$) [35], ($\nu=2,\mu=1$) [21], and ($\nu=1,\mu=2$) [20]. For this investigation the exponents $\nu=1$ and $\mu=2$ were used following from previous studies of shape [13]. A schematic representation of the model is shown in Fig. 1, where the definition of γ is the same as in Ref. [26].

B. Simulations

The distance dependence of the potential energy calculated from the Gay-Berne potential for side-to-side and end-to-end configurations of all models with respect to one an-

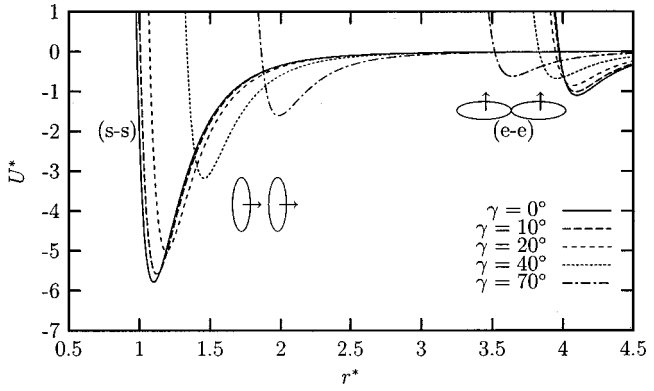

FIG. 2. The distance dependence of the potential energy calculated from the Gay-Berne potential for side-to-side (s-s) and end-to-end (e-e) configurations of all bent-core models with respect to one another. The arrow represents the direction of the steric dipole for $\gamma > 0°$.

other is shown in Fig. 2. As the deviation is increased from the rodlike case ($\gamma = 0°$) the minimum of the potential energy becomes less negative up to $\gamma = 70°$ for the side-to-side configuration as seen in Fig. 2. The intermolecular separation at which the minimum occurs in the side-to-side configuration steadily increases with increase in the molecular angle γ. In contrast, the intermolecular separation at which the minimum occurs in the end-to-end configuration decreases steadily as γ increases. This is due to the ''wings'' of the bent-core shape preventing close alignment. This effect is understood by examining the potential energy contours for parallel two-site molecules interacting via the Gay-Berne potential as a function of their separation, orientation, and angle between the sites, as shown in Figs. 3(a–e). A small deviation is initially seen as γ increases from 0° to 10°, with a bent-core shape appearing in Fig. 3(b). As $\gamma = 20°$ is reached as shown in Fig. 3(c), the bent-core shape is more pronounced. Figure 3(d) with $\gamma = 40°$ demonstrates that the shape where the still bent-core is tending to a shorter, wider model, whilst at $\gamma = 70°$ [Fig. 3(e)], the shape has become markedly wider and shorter, with a length-to-breadth ratio of less than 2:1. It is interesting to note that as γ increases the biaxiality of the molecular models also increases. These potential plots also provide insight into the shifting of the pair potential minima to increasingly lower values of the intermolecular separation for the end-to-end configuration as γ increases. Because the site-site separation is kept constant, as γ increases, the molecules length-to-breadth ratio becomes less and the molecules can, therefore, approach closer to each other in the end-to-end configuration but are further separated in a side-to-side configuration. This decrease in the length-to-breadth ratio is seen in the real molecules. Niori and co-workers [5] have shown how the angle of bend of the bent-core molecules decreases as T^* is lowered. Hence the model systems extend over the range of angles found in real molecules of $\gamma = 45°$ to $\gamma = 80°$.

The molecular dynamics simulation study reported here was undertaken in the isothermal-isobaric (N-P-T) ensemble using systems of $N = 1024$ particles in a rectangular box, sides of fixed ratio 1:1:2 with periodic boundary conditions. The simulations were undertaken in the N-P-T ensemble to best reflect realistic conditions and allow for comparison with experimental results. The details of the isothermal-isobaric molecular dynamics simulation followed Brown and Clarke [36] and have been reported elsewhere [13]. A reduced pressure P^* $(\equiv P\sigma^3/\epsilon_o)$ of 2.0 was used for all simulations and the system cooled from an isotropic system to the solid phase in steps of T^* $(\equiv kT/\epsilon_0) = 0.1$. To increase the speed of computation a potential cutoff of $r^* = 5.5$ along with a Brode-Aldrichs [37] neighbor list radius of $r^* = 5.8$ was used. A reduced time step of $\Delta t^* = 0.0005$ was used, reduced to $\Delta t^* = 0.00\,015$ when approaching a phase transition point, where $\Delta t^* \equiv \Delta t(m\sigma_0^2/\epsilon_o)^{1/2}$. The number of simulation steps varied between 4×10^5 and 2×10^6.

The orientational order was analyzed using standard methods described in Refs. [38,39]. The tensor $\mathbf{Q}^{xx}$ is defined by

$$Q^{xx}_{\alpha\beta} = \frac{1}{N}\sum_{i=1}^{N}\frac{3\hat{x}_{i\alpha}\hat{x}_{i\beta} - \delta_{\alpha\beta}}{2}, \tag{8}$$

where $\hat{x}_i$ is a unit vector pointing along one axis of molecule i; $\mathbf{Q}^{yy}$ and $\mathbf{Q}^{zz}$ are defined similarly in terms of unit vectors $\hat{y}_i$ and $\hat{z}_i$ pointing along the other molecular axes. To obtain a system director, the dominant eigenvalue of each of $\mathbf{Q}^{xx}$, $\mathbf{Q}^{yy}$, and $\mathbf{Q}^{zz}$ was found, and the system director was identified with the eigenvector associated with the largest of these dominant eigenvalues; if necessary, the molecular axes were relabeled so that this was an eigenvalue of $\mathbf{Q}^{zz}$. This direction defined a unit vector along the Z axis. The order parameter Q^2_{00} is then defined as $\langle \mathbf{Z}\cdot\mathbf{Q}^{zz}\cdot\mathbf{Z}\rangle$, which coincides with the usual nematic order parameter P_2 if we regard the molecule's z axis as the molecule director, so we see that Q^2_{00} is zero for an isotropic system, and rises to unity for a perfectly ordered one. To identify the Y axis, we considered the largest dominant eigenvalue of $\mathbf{Q}^{xx}$ and $\mathbf{Q}^{yy}$, with the associated eigenvector; again, relabeling the molecular axes, if necessary, so that this direction was given by an eigenvector of $\mathbf{Q}^{yy}$. As this direction was not, in general, orthogonal to the Z axis, it was projected to the plane orthogonal to Z to give the Y axis. Finally, the X axis was simply chosen to complete this to a right-handed system.

There are two measures of biaxiality, which might be considered. First, we consider that used in Ref. [39]:

$$Q^2_{22} = \frac{1}{3}\langle X\cdot Q^{xx}\cdot X + Y\cdot Q^{yy}\cdot Y - X\cdot Q^{yy}\cdot X - Y\cdot Q^{xx}\cdot Y\rangle. \tag{9}$$

This measures the extent to which the x and y molecular axes are ordered in the plane orthogonal to the system director Z. A second measure of biaxiality is given by the difference between the two minor eigenvalues of $\mathbf{Q}^{zz}$ as outlined in Ref. [40]. Diagonalizing $\mathbf{Q}^{zz}$ we have

$$\mathbf{Q}^{zz} = \begin{pmatrix} q^{zz}_{xx} & 0 & 0 \\ 0 & q^{zz}_{yy} & 0 \\ 0 & 0 & q^{zz}_{zz} \end{pmatrix}, \tag{10}$$

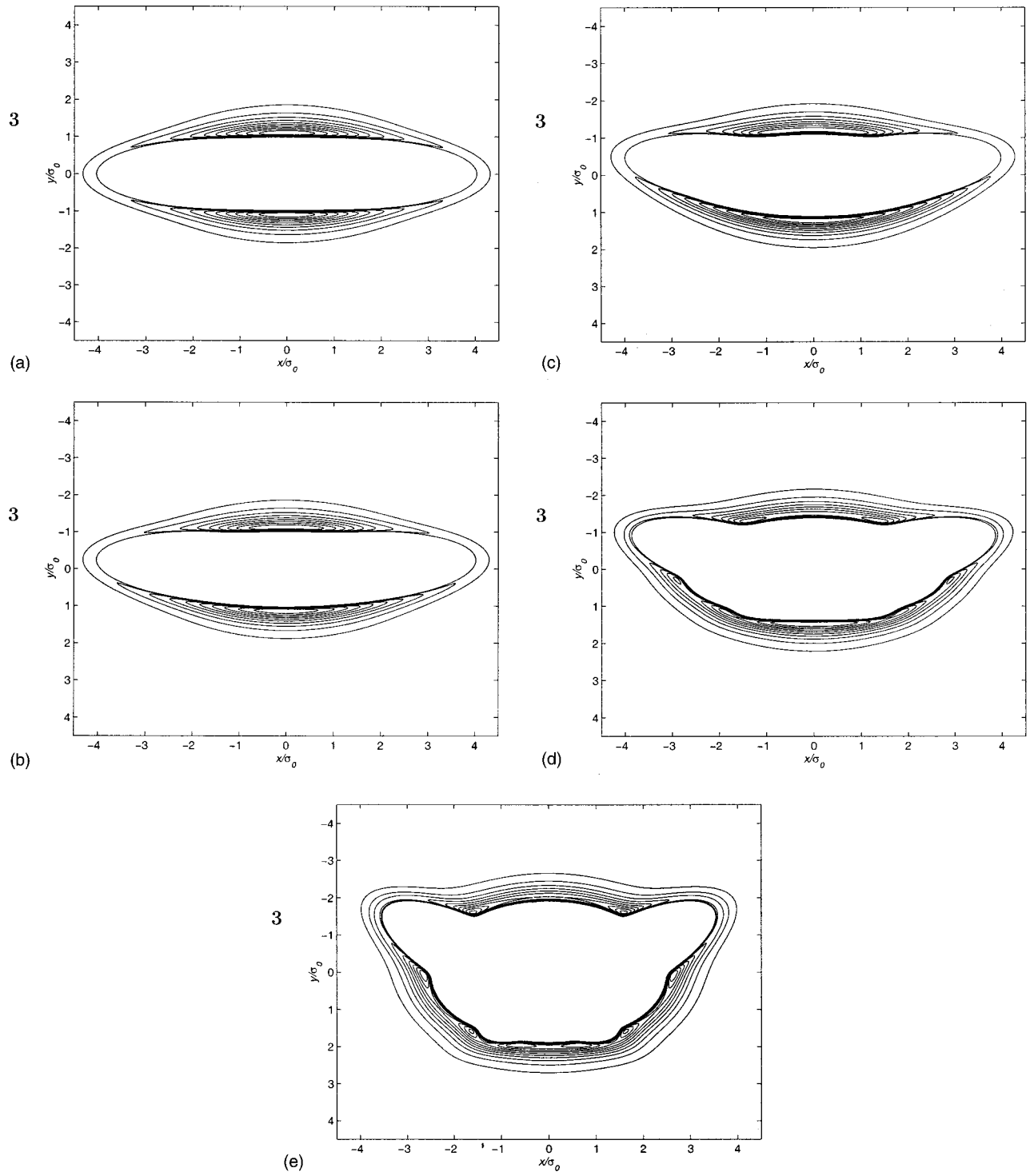

FIG. 3. Potential energy contours calculated for parallel molecules interacting via the Gay-Berne potential as a function of intermolecular separation (coordinates of x and y are expressed in units of σ_0) and their orientation with respect to the intermolecular vector for (a) $\gamma=0°$, (b) $\gamma=10°$, (c) $\gamma=20°$, (d) $\gamma=40°$, and (e) $\gamma=70°$.

where $|q_{zz}^{zz}|>|q_{yy}^{zz}|>|q_{xx}^{zz}|$. Recalling that q_{zz}^{zz} is Q_{00}^2 and the trace of Q_{00}^2 is zero, we can write this as

$$\mathbf{Q}^{zz}=\begin{pmatrix} -Q_{00}^2/2-\xi & 0 & 0 \\ 0 & -Q_{00}^2/2+\xi & 0 \\ 0 & 0 & Q_{00}^2 \end{pmatrix}. \qquad (11)$$

For an uniaxial system $q_{yy}^{zz}=q_{xx}^{zz}$, the molecule directors are equally likely to deviation in any direction from the system director. If the two are unequal, i.e., if $\xi\neq 0$, then the molecule directors determine a preferred plane, and so the system exhibits a type of biaxiality different from that measured by Q_{22}^2. These biaxiality measures will be used in the discussion in Sec. IV. In addition, in order to investigate steric

''polar'' order within the layers we can define a steric ''polar'' order parameter $\langle P_1 \rangle$ that defines the degree to which the transverse steric dipole axis is aligned from

$$\langle P_1 \rangle = \frac{1}{N} \sum_{i=1}^{N} \hat{\mathbf{y}}_i \cdot \hat{\mathbf{Y}}.$$

Structural information was obtained via the orientational averaged pair distribution function $g(r^*)$, the longitudinal, $g_\parallel(r_\parallel^*)$, and transverse, $g_\perp(r_\perp^*)$, pair distribution functions,where $r^* \equiv r/\sigma_o$.

$$g(r) = \frac{V}{N^2} \left\langle \left(\sum_i \sum_{j \neq i} \delta(\mathbf{r} - \mathbf{r}_{ij}) \right) \right\rangle, \tag{12}$$

$$g_\parallel(r_\parallel) = \frac{V}{N^2} \left\langle \left(\sum_i \sum_{j \neq i} \delta|(\mathbf{r} - \mathbf{r}_{ij}) \cdot \hat{\mathbf{Z}}| \right) \right\rangle, \tag{13}$$

$$g_\perp(r_\perp) = \frac{V}{N^2} \left\langle \left(\sum_i \sum_{j \neq i} \delta|(\mathbf{r} - \mathbf{r}_{ij}) \times \hat{\mathbf{Z}}| \right) \right\rangle. \tag{14}$$

A spherical cutoff was used for $g(r^*)$ and a cylindrical volume was used in the calculation of $g_\parallel(r_\parallel^*)$ and $g_\perp(r_\perp^*)$, the axis of the cylinder being aligned along the director $\hat{\mathbf{Z}}$. Use of a cylindrical geometry in this way enabled the structure within and between the layers to be examined.

III. SIMULATION RESULTS AND DISCUSSION

Results are presented for the rodlike model and for a series of bent-core models. Starting from the isotropic phase, the systems were cooled in steps of $T^* = 0.1$ or $T^* = 0.2$, the former used if the system was close to a phase transition. The pressure was kept constant at $P^* = 2.0$ and the simulations continued at each point until consecutive simulation runs resulted in identical thermodynamic values, within limits of error. The cooling runs stopped once the system had reached a near solid state, determined from the second-rank orientational order parameter Q_{00}^2.

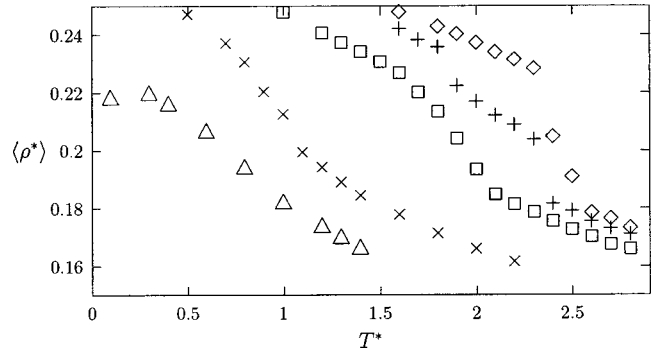

FIG. 4. Average scaled density $\langle \rho^* \rangle$ as a function of scaled temperature T^* for the rod ($\diamond$), and bent-core $\gamma = 10°$ (+), $\gamma = 20°$ ($\square$), $\gamma = 40°$ ($\times$), and $\gamma = 70°$ ($\triangle$) models for $N = 1024$.

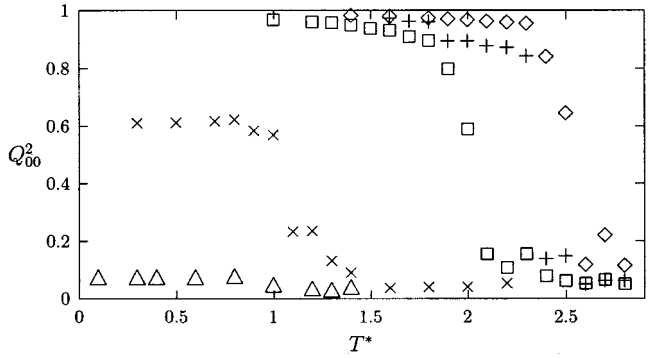

FIG. 5. Average second-rank orientational order parameter Q_{00}^2 as a function of scaled temperature T^* for the rod ($\diamond$), and bent-core $\gamma = 10°$ (+), $\gamma = 20°$ ($\square$), $\gamma = 40°$ ($\times$), and $\gamma = 70°$ ($\triangle$) models for $N = 1024$.

A. Rodlike model

Figure 4 shows the variation in density as the systems were cooled and Fig. 5 shows the corresponding variation in the second-rank orientational order parameter Q_{00}^2 for $\gamma = 0°$, 10°, 20°, 40°, and 70°.

Three separate phase transitions were seen to occur in the rod model. The system is seen to be isotropic at temperatures above $T^* = 2.5$, the average order parameter Q_{00}^2 showing little more fluctuations due to finite system size. The radial pair distribution function $g(r^*)$ and the longitudinal pair distribution functions $g_\parallel(r_\parallel^*)$, show no structure, as we would expect for the isotropic phase.

As the system is cooled a discontinuity occurs in the density at $T^* = 2.5$, indicating a phase transition. The average value of Q_{00}^2 at $T^* = 2.5$ increases to 0.641 ± 0.021 from 0.115 ± 0.034 at $T^* = 2.6$. No structure is seen in the longitudinal pair distribution function (Fig. 6) identifying the presence of a nematic phase. This simulation was continued for 1.6×10^6 time steps to confirm its stability.

When the temperature is lowered further to $T^* = 2.4$ we again see a phase transition with a discontinuity in the density and an associated increase in the order parameter to a value of 0.837 ± 0.162. Figure 6 shows an oscillation in the longitudinal pair distribution function $g_\parallel(r_\parallel^*)$. This shows the presence of a layered structure in the system. However, the low amplitude oscillations indicate a poorly defined layered

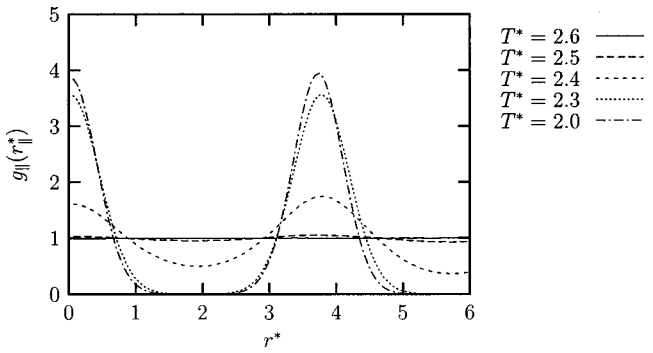

FIG. 6. Pair distribution functions for rodlike model resolved parallel to the director for a range of temperatures.

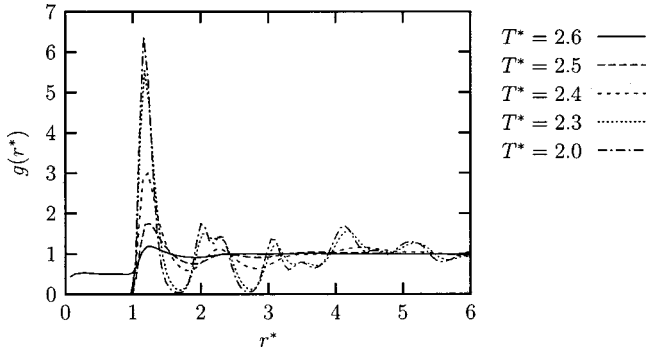

FIG. 7. Pair distribution functions for rodlike model for a range of temperatures.

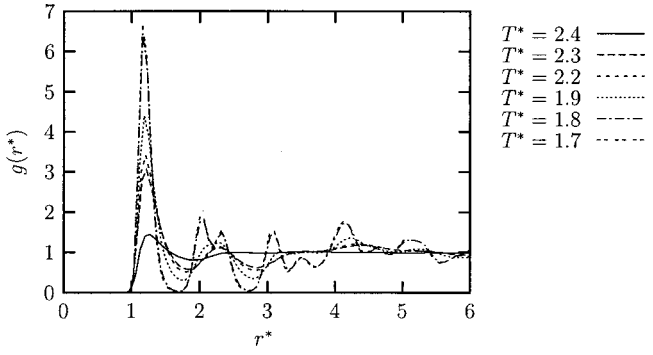

FIG. 9. Pair distribution functions for $\gamma = 10°$ bent-core model for a range of temperatures.

system. As T^* is reduced further to 2.3, a third transition is seen in the density in Fig. 4. The second-rank orientational order parameter increases to a value of $Q_{00}^2 = 0.951 \pm 0.002$. Examination of the pair distribution function in Fig. 6 reveals a change in the layer structure of the system. The increased amplitude of the peaks of $g_\parallel(r_\parallel^*)$ shown in Fig. 6 indicate that the layers have become much more defined. The split of the second peak in $g(r^*)$, Fig. 7, at $r^* = 2.03$ and $r^* = 2.29$ reduced units is indicative of a smectic-*B* phase.

The smectic-*B* phase persisted for all temperatures studied below $T^* = 2.3$.

B. $\gamma = 10°$ and $\gamma = 20°$

As the system with $\gamma = 10°$ is cooled, a discontinuity is observed in the density at $T^* = 2.3$ as shown in Fig. 4. Above this temperature the system is an isotropic fluid with values of Q_{00}^2 less than 0.148 ± 0.036, shown in Fig. 5. No structure is seen in the pair distribution functions. A discontinuity occurs in the density at $T^* = 2.3$ and at the same time the orientational order parameter Q_{00}^2 increases to 0.843 ± 0.004. However, an oscillation in the longitudinal pair distribution function $g_\parallel(r_\parallel^*)$ shown in Fig. 8 also occurs at this temperature. Hence a smectic phase is identified for the $\gamma = 10°$ model as opposed to the nematic phase found in the simulation of the $\gamma = 0°$ model. The absence of structure in the radial pair distribution function $g(r^*)$ (Fig. 9), shows this to be a smectic-*A* phase.

For $\gamma = 20°$ a discontinuity is seen in ρ^* at $T^* = 2.0$ and Q_{00}^2 rises to a value of 0.596 ± 0.015. No oscillation occurs in $g_\parallel(r_\parallel^*)$, as shown in Fig. 10, at this temperature so a nematic phase is identified. The simulation was continued for 1.4×10^6 steps to confirm its existence. As the temperature was lowered to $T^* = 1.9$ a rise in the order parameter, Q_{00}^2, to 0.793 ± 0.011 was seen accompanied by a discontinuity in the density. An oscillation was seen in the longitudinal pair distribution function $g_\parallel(r_\parallel^*)$, which is indicative of a layered system. Similarly to the $\gamma = 10°$ model, an absence of a split in the second peak of $g(r^*)$, Fig. 11, identifies this as a smectic A phase.

Comparison of the simulations of $\gamma = 0°$, $\gamma = 10°$, and $\gamma = 20°$ indicates a trend of decreasing temperature of transition from the isotropic to the ordered phase is seen, but the ordered phase differs from a nematic for $\gamma = 0°$ to a smectic *A* for $\gamma = 10°$ and and a nematic for $\gamma = 20°$ indicating the subtle effect of varying the transverse steric dipole.

A further transition occurs at $T^* = 1.8$ for the $\gamma = 10°$ model and $T^* = 1.6$ for the $\gamma = 20°$ model with Q_{00}^2 rising to 0.960 ± 0.002 and 0.924 ± 0.004, respectively. Observation of $g_\parallel(r_\parallel^*)$ at these temperatures, Figs. 8 and 10, respectively, show an increase in the amplitude of the oscillations due to better definition of the layers in the phase. A split in the second peak of the radial pair distribution function shown in Figs. 9 and 11 for $\gamma = 10°$ and 20°, respectively, corresponds to the presence of a smectic-*B* phase in both cases. For the $\gamma = 10°$ model, the split peak occurs between $r^* = 2.01$ and

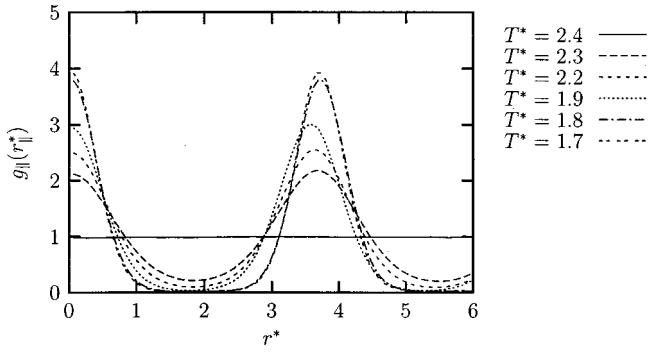

FIG. 8. Pair distribution functions for $\gamma = 10°$ bent-core model resolved parallel to the director for a range of temperatures.

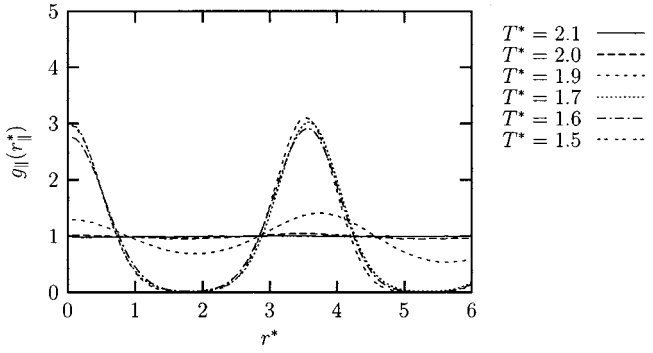

FIG. 10. Pair distribution functions for $\gamma = 20°$ bent-core model resolved parallel to the director for a range of temperatures.

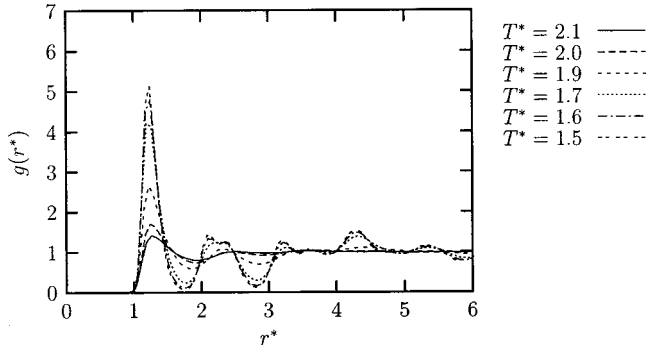

FIG. 11. Pair distribution functions for $\gamma = 20°$ bent-core model for a range of temperatures.

$r^* = 2.33$ and, for the $\gamma = 20°$, between $r^* = 2.10$ and $r^* = 2.36$. This transition is comparable with that found for the $\gamma = 0°$ model at $T^* = 2.3$. In the case of the $\gamma = 20°$ model the transition was not as clear from the radial pair distribution functions as for the $\gamma = 10°$ model. To more accurately determine the temperature of the transition in the $\gamma = 20°$ model and to investigate the possibility of steric polar order within the layers a single layer was examined visually. By rotating the view so that the observer is looking down the director it is possible to determine whether any hexagonal packing is present and, therefore, whether the phase is a smectic *A* or a smectic *B*. Two snapshots are shown in Figs. 13 and 14 for the $\gamma = 20°$ model, one at $T^* = 1.7$ (before the transition), and one at $T^* = 1.6$ (after the transition), respectively. It can be seen in Fig. 13 that before the transition some short range hexagonal order exists. After the transition, at $T^* = 1.6$, the hexagonal order is present throughout the layer indicating the presence of a smectic-*B* phase. Both Figs. 13 and 14 show no overall steric polar order illustrated by the lack of an overall direction for the line vectors representing the direction of the steric ''polar'' axis. This result was confirmed by an analysis of the steric ''polar'' order parameter $\langle P_1 \rangle$ in the plane, which showed no significant magnitude. No overall ''polar'' order was found in the rodlike, $\gamma = 10°$ or the $\gamma = 20°$ models and, in addition, when adjacent layers were analyzed, no antiparallel ''polar'' order

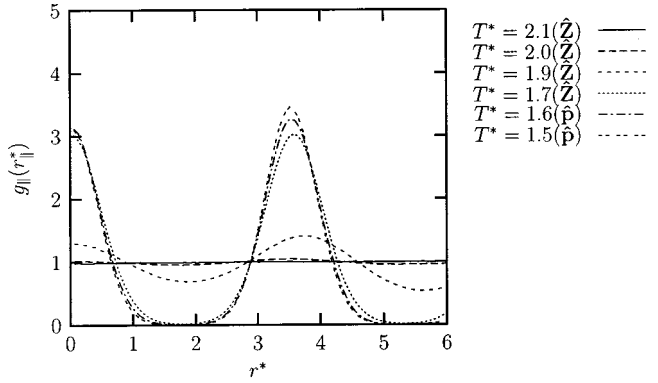

FIG. 12. Pair distribution functions for $\gamma = 20°$ bent-core model resolved parallel to (a) the director $\hat{\mathbf{Z}}$, and (b) the layer normal $\hat{\mathbf{p}}$, for a range of temperatures, the latter including the results of the simulated annealing.

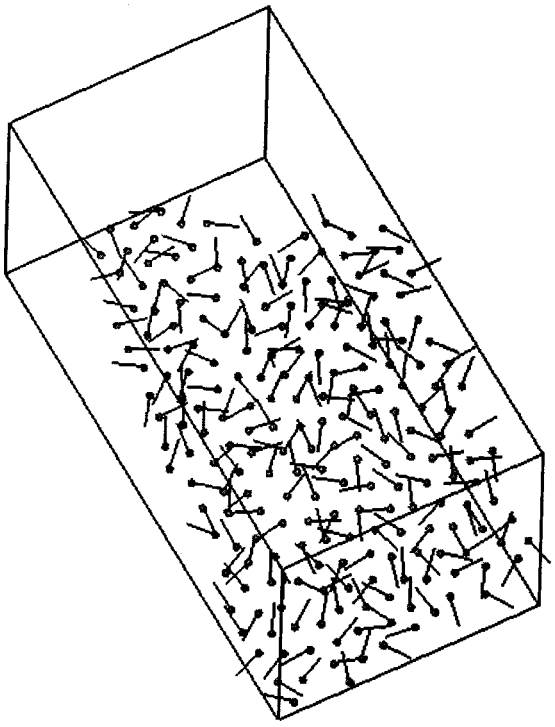

FIG. 13. A snapshot of a single layer from the production run at $T^* = 1.7$ for the $\gamma = 10°$ bent-core model. The spheres represent the centers of mass of the particles and the line vector, $-$, indicates the direction of the steric polar axis.

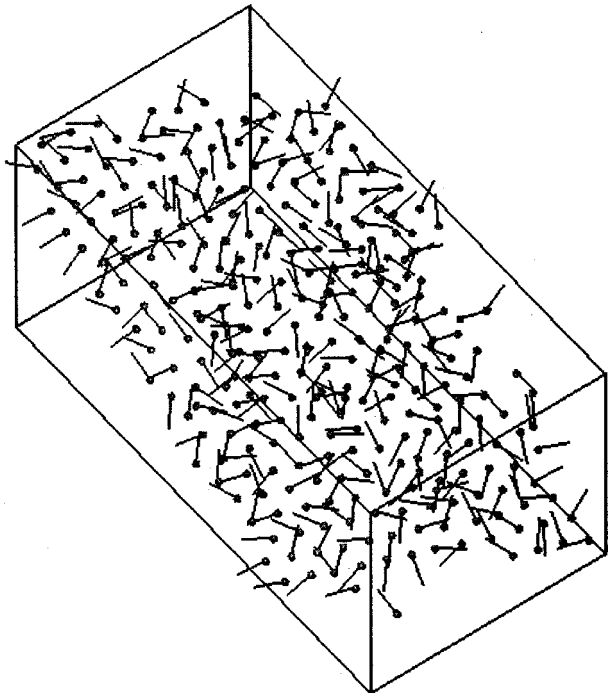

FIG. 14. A snapshot of a single layer from the production run at $T^* = 1.6$ for the $\gamma = 10°$ bent-core model. The spheres represent the centers of mass of the particles and the line vector, $-$, indicates the direction of the steric polar axis.

TABLE I. Results from the simulated annealing analysis for the $\gamma=20°$ bent-core model showing the average angle between the system director and the layer normal, $\cos^{-1}(\hat{\mathbf{Z}}\cdot\hat{\mathbf{p}})$.

T^*	Tilt (deg)
2.0	
1.9	
1.8	
1.7	
1.6	3.30 ± 0.94
1.5	5.87 ± 0.93
1.4	10.37 ± 0.43
1.3	10.86 ± 1.02
1.2	12.49 ± 5.68
1.0	11.23 ± 1.09

was found to be unlike many real bent-core molecules. The origin of such order may lie in the transverse electric dipole present in real molecules and absent in these steric models. Ferroelectric order has been found in a current study by the authors [34], which includes a transverse electric dipole in the model.

An interesting feature found to be present in the $\gamma=10°$ model is the increase in the layer spacing in the final transition from the smectic-*A* phase to the smectic-*B* phase at $T^*=1.8$ shown in Fig. 8. A second interesting feature for the $\gamma=20°$ model is found in the longitudinal pair distribution functions. They show a decrease in the amplitude of oscillation as the system cools in the smectic-*B* phase, from $T^*=1.7$ to $T^*=1.6$, as shown in Fig. 10. These are unusual results, since it is generally expected that as the density increases the layer spacing decreases and the amplitude of the oscillations in the longitudinal pair distribution functions increase. In the case of the $\gamma=10°$ model it is likely that the bent-core shape is preventing intercalation of the layers as the smectic-*B* phase is reached. As the bent cores come in close proximity, steric factors prevent close alignment in the direction of the long molecular axis within the layer. The decreased amplitude, seen in the $\gamma=20°$ model, in the longitudinal pair distribution function is a feature seen in tilted systems. Further analysis was undertaken to confirm this case and to establish whether there are any underlying substructures in the phase. This was initially accomplished by determining whether the molecules had become tilted with respect to the layer normal. This was accomplished using a simulated annealing method to find a better layer normal $\hat{\mathbf{p}}$, than provided by the system director $\hat{\mathbf{Z}}$ [41,42]. The $\gamma=10°$ model was found to have no in-layer tilt of the molecules, however, the results of the simulated annealing for the $\gamma=20°$ model, shown in Fig. 12 for the temperatures $T^*=1.6$ and $T^*=1.5$, are indicative of a tilted phase. The structure of the longitudinal pair distributions $g_{\parallel}(r_{\parallel}^*)_{\hat{\mathbf{p}}}$ given by

$$g_{\parallel}(r_{\parallel})_{\hat{\mathbf{p}}}=\frac{V}{N^2}\left\langle\left(\sum_i\sum_{j\neq i}\delta|(\mathbf{r}-\mathbf{r}_{ij})\cdot\hat{\mathbf{p}}|\right)\right\rangle, \qquad (15)$$

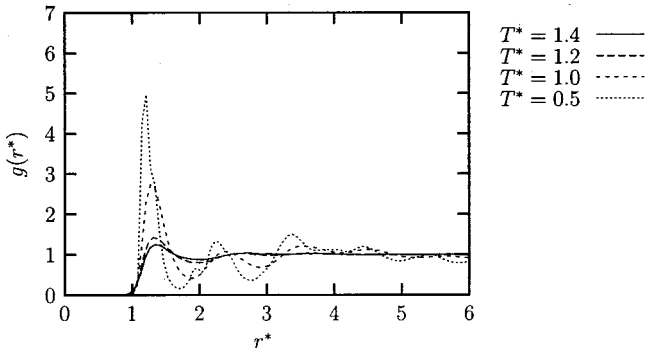

FIG. 15. Pair distribution functions for $\gamma=40°$ bent-core model for a range of temperatures.

after the simulated annealing showed an increased amplitude of oscillation compared to $g_{\parallel}(r_{\parallel}^*)_{\hat{\mathbf{Z}}}$ [Eq. (13)]. This confirms that the simulated annealing analysis had determined a layer normal $\hat{\mathbf{p}}$ in a different direction to the system director $\hat{\mathbf{Z}}$. Hence the final phase transition for the $\gamma=20°$ model occurs between a smectic-*A* phase and a tilted smectic-*B* phase at $T^*=1.6$. Table I shows the average tilt angle for all the tilted phases for the $\gamma=20°$ model for values of $T^*=1.6$ and below. The tilt occurred at $T^*=1.6$, hence all the smectic-*B* phases that formed for the $\gamma=20°$ model were tilted with angles increasing from $3.3°\pm1.0$ at $T^*=1.6$ to $12.5°\pm5.7$ at $T^*=1.2$ then decreasing to $11.2°\pm1.1$ at $T^*=1.0$. This is a low range compared with the range of angles of between approximately 25° and 35°, e.g., Refs. [7,43] found in real bent-core phases. The molecule's synclinic tilting breaks symmetry with steric interactions alone, as observed by Xu *et al.* [28], however, it is not a chiral system. A potential problem of the imposition of fixed aspect ratio is that it could affect the equilibrium layer spacing. However, this would be indicated by an anisotropy in the pressure tensor that is absent in these studies.

C. $\gamma=40°$

As the system was cooled, the first transition occurred at a temperature of $T^*=1.0$, a considerably lower temperature than that seen in the earlier models. This transition is seen in the discontinuity in $\langle\rho^*\rangle$ shown in Fig. 4 and the increase in the order parameter Q_{00}^2, to 0.569, as shown in Fig. 5. The longitudinal pair distribution function $g_{\parallel}(r_{\parallel}^*)$, shown in Fig. 16, is featureless as is $g(r^*)$ in Fig. 15. However, visual inspection revealed a striped system of smectic layers rotated with respect to one another. The total rotation across the cell must be a multiple of 2π. In order to investigate the effect of the periodic boundary conditions the system was doubled in size to $N=2048$ and cooled through the transition from $T^*=1.1$, where there was no striped phase to $T^*=1.0$. Again striped domains were observed and the same discontinuity was seen in $\langle\rho^*\rangle$ and the value of Q_{00}^2 was increased to 0.4 this time rather than 0.6, as seen for the $N=1024$ system.

In this phase we find that the biaxiality measure ξ is nonzero, as shown in Fig. 17, indicating a preferred plane for the molecule directors. A snapshot of the $N=2048$ molecular

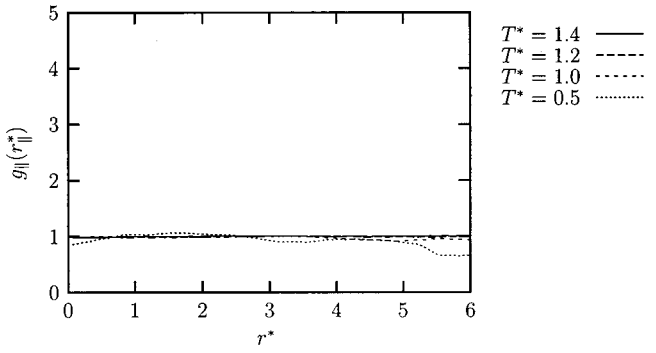

FIG. 16. Pair distribution functions for $\gamma = 40°$ bent-core model resolved parallel to the director for a range of temperatures.

system shown in Fig. 18 indicates a striped structure similar to a twist grain boundary (TGB) phase. The figures indicate that each striped region has a high degree of orientational order; the relatively low order parameter for the system is caused by the different regions having different directors. This is corroborated by a computation of the order parameter Q^2_{00} in increasing neighborhoods of each molecule in the system, as shown in Fig. 19. We see that for a sufficiently small neighborhood of each molecule the order parameter is high, but it drops when the neighborhood becomes large enough to include molecules from a different stripe. By comparison, for the $\gamma = 0°$ system, where no striping is evident, the order parameter does not decrease as the neighborhood is increased. Further evidence of the striped regions is provided by a consideration of $g_{\|}(r^*_{\|})_{local}$ for a cylinderlike structure where the diameter and height of the cylinder vary, as shown in Fig. 20. The local longitudinal pair distribution function is defined as [13]

$$g_{\|}(r_{\|})_{local} = \frac{V}{N^2}\left\langle \left(\sum_i \sum_{j \neq i} \delta|(\mathbf{r} - \mathbf{r}_{ij}) \cdot \hat{\mathbf{u}}_i| \right) \right\rangle, \qquad (16)$$

with respect to the direction $\hat{\mathbf{u}}_i$ of molecules locally. Increasing the height of the cylinder increased the amplitude of the oscillation in $g_{\|}(r^*_{\|})$ as the layers above and below are correlated. In contrast, increasing the diameter of the cylinder reduces the amplitude of oscillation as the correlation takes into account molecules in the next striped domain.

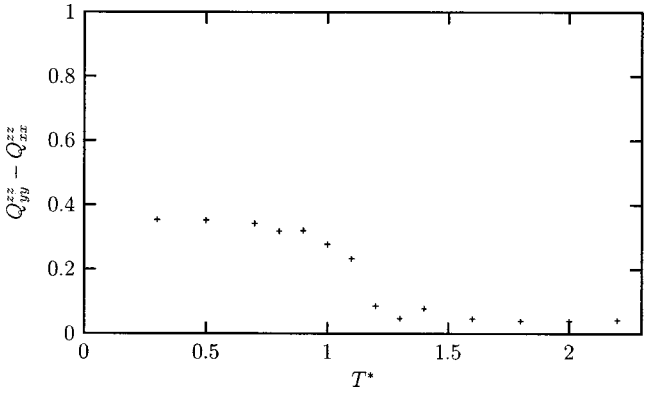

FIG. 17. Difference in the minor eigenvalues $Q^{zz}_{yy} - Q^{zz}_{xx}$ for $\gamma = 40°$ as a function of reduced temperature T^*.

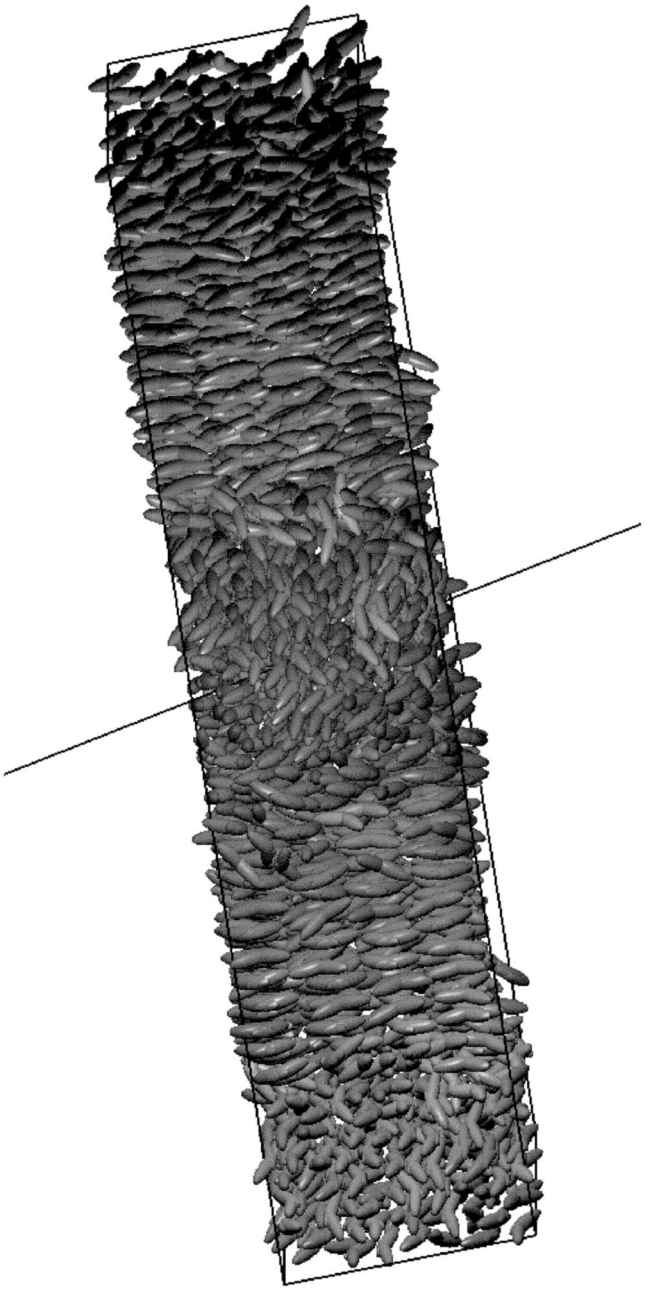

FIG. 18. A snapshot from the production run at $T^* = 1.0$ for the $\gamma = 40°$ bent-core model with $N = 2048$ molecules. The system director is identified by the long line through the center of the box.

This result is mirrored in the behavior of real bent-core molecules. Sekine *et al.* [46] describe a bent-core system in the smectic-blue phase that consists of layered domains twisted with respect to one another. Each domain is ferroelectric and the rotation of each domain with respect to the next is about the polar axis of the molecule. Although the present system shows no ferroelectric ordering the layered domain structure is similar to that reported in Ref. [46].

The biaxiality indicated by the nonzero value of ξ is a consequence of the striped structure. Within each stripe, the molecules have a high degree of orientational order, and the

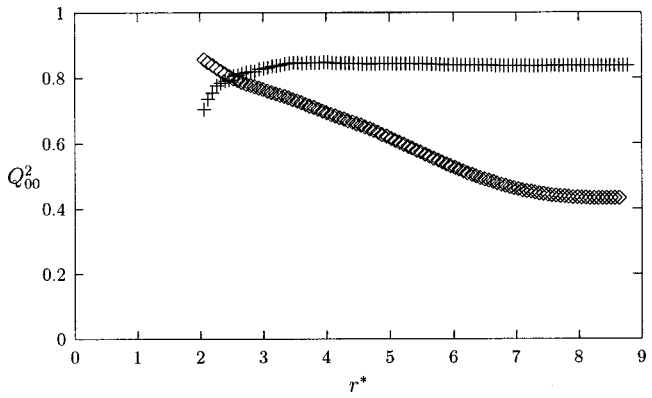

FIG. 19. Second-rank orientational order parameter as a function of intermolecular separation for the $\gamma=40°$ ($\diamond$) and $\gamma=0°$ (+) models.

director for each stripe lies in a common plane. Because the stripes are of different thicknesses and their directors are approximately at right angles to one another, we obtain a system director that lies in the common plane of the directors for each stripe. The molecule directors are scattered about this system director, but as they have a strong tendency to lie in this common plane, we obtain a significant value for ξ. Thus in this ''TGB-like'' phase, the biaxiality measure ξ is actually caused by the presence of highly ordered domains with different directors lying in a common plane. The other biaxiality parameter Q_{22}^2, is approximately zero, since even within each domain the minor molecular axes show no preferred direction. Thus, although the phase does exhibit two preferred directions, and so, by definition of biaxiality, the molecular minor axes are not significantly ordered.

Further cooling does not result in any further phase transitions. The pair distribution functions continue to show the same ''TGB-like'' phase as already described. An interesting feature occurs in the second peak in the pair distribution function $g(r^*)$ at $T^*=0.5$ shown in Fig. 15 when a shoulder appears at $r^*=2.0$. Since the length-to-breadth ratio of the model is 3:1 this may be due to ''T'' configurations between striped domains. A similar feature was seen in the pair distribution functions [44,45] in computer simulations of benzene and napthalene where such configurations are common.

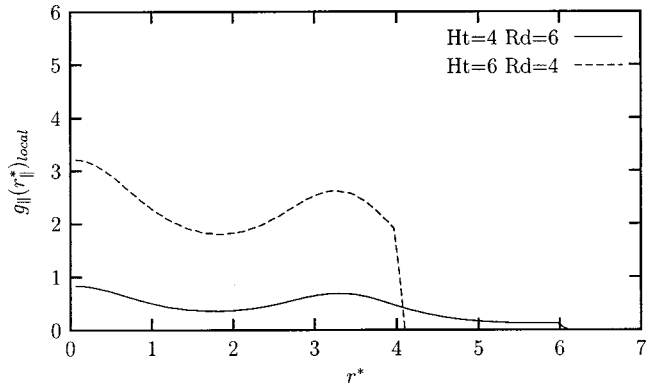

FIG. 20. Pair distribution functions for $\gamma=40°$ bent-core model resolved parallel to the local director for two different cylinder dimensions.

D. $\gamma=70°$

This model has an angle that most closely resembles the real molecules but its length-to-breadth ratio is less realistic. Examination of the density and Q_{00}^2 as a function of temperature, shown in Figs. 4 and 5 show no transition to an ordered phase. As the temperature is decreased, the density increases as expected, however, the value of Q_{00}^2 gives no indication of a liquid crystal phase. Similarly, the distribution functions show no structure at any temperature. It is most likely the case, considering Fig. 3(e), that the model used here to approximate the bent-core molecular shape fails as the value of γ reaches a critical value. It appears that the $\gamma=70°$ model has formed interlocking pairs and is frozen into a plastic state. This is given further credence by the absence of any change in the value of the second-rank orientational order parameter at temperatures lower than $T^*=0.6$.

IV. CONCLUSIONS

We have undertaken computer simulation studies of bent-core molecules using a two-site Gay-Berne potential. The range of angles studied was from the rodlike, $\gamma=0°$ to $\gamma=70°$, systems comparable with angles attained in real bent-core molecules, which result in an increasing transverse steric dipole.

The bent-core shape was seen to affect the type of phase formed as the systems were cooled. With no angle of bend, $\gamma=0°$, a nematic phase was seen. However, with the introduction of a small degree of bend in the molecules, $\gamma=10°$, no nematic (N) phase was seen and a transition from the isotropic liquid straight to a smectic-A phase occurred. A trend was established where an increase in the angle of bend γ, and hence increased transverse steric dipole results in a decreased temperature of transition to the first ordered phase. The first ordered phase varied as γ was increased from N $\rightarrow$Sm$A\rightarrow$N$\rightarrow$ TGB-like as γ was increased; no ordered phase was found at $\gamma=70°$.

An interesting finding was the appearance of a TGB-like phase for the $\gamma=40°$ model at low temperatures. As already described [46], this is a result that is seen in experimental studies of the real molecules with a blue TGB phase. It, therefore, appears that the bent-core shape does influence the appearance of the real phases of the molecules even in the absence of polar forces.

For the highest value of γ studied here no ordered phase was formed. With such a high degree of bend in the model, the length-to-breadth ratio becomes rather unrealistic and it is little surprising that no liquid crystal phases were formed. Increasing the overall length-to-breadth ratio of the molecule will allow larger angles to be studied.

More complex in-layer and interlayer packing was found in simulations of the $\gamma=10°$ and $\gamma=20°$ models. In the case of the $\gamma=10°$ bent-core system, close alignment of the bent cores was prevented in the smectic-B phase resulting in an increased layer separation in the phase. No tilting of the layers was found and the increased separation was attributed to steric effects. The $\gamma=20°$ model formed a tilted smectic-B phase, identified through the simulated annealing method.

The angle of tilt, defined as the angle between the layer normal and the system director was seen to vary between $3.3° \pm 1.1$ and $12.5° \pm 5.7$. Tilted phases are often seen in the real bent-core systems, however, no clinicity is seen in the smectic-*B*-type phase found in the real bent-core molecules.

Adjacent layers were separated to determine whether any difference occurred in alternate layers, a difference that is of key importance in the real bent-core molecules. No alignment of the steric dipole axis was found in either the $\gamma = 10°$ and $\gamma = 20°$ models, determined by the $\langle P_1 \rangle$ order parameter; no difference in the direction of tilt was detected in the $\gamma = 20°$ model, determined by the angle between the directors of the separated layers.

The results presented here have shown the subtle effect on phase behavior of increasing the transverse steric dipole. Initially the nematic phase is destabilized with respect to the smectic-*A* phase. However, the transverse bent-core shape is seen to have a disrupting effect on the system; higher angles of bend result in the reappearance of the nematic phase, a TGB-like phase, and finally the complete suppression of ordered phases. For low values of γ the smectic-*A* to smectic-*B* phase transition occurs, however, disruption of the smectic layering occurs in two ways dependent on the value of γ. For the lowest value of γ, layer spacing increases to accommodate the bent-core shape within the smectic layering. As γ is increased the molecules tilt with respect to the smectic layer normal to the smectic-*A*–smectic-*B* phase transition.

Two common features seen in the real bent-core molecules have been reproduced in this study. The first is the rare occurrence of a nematic liquid crystal phase in the phase diagram. This has been reproduced with no nematic phases for the $\gamma = 10°$ and $\gamma = 40°$ bent-core models; the $\gamma = 20°$ model displayed a nematic phase at a single point. Nematic phases have been observed in real materials but are rare. The second common feature is the tilt of the molecules with respect to the layer normal; this was seen in the $\gamma = 20°$ bent-core model. This is of importance when polar ordering is present in the system since this can lead to an overall reduction of the phase symmetry and the production of chiral phases. Two kinds of structures are often seen with regard to the tilting of the molecule, synclinic, and anticlinic structures. No significant difference was seen in the directors of adjacent layers of molecules in the tilted smectic-*B* phase indicating that a synclinic structure alone was present. The TGB-like phase of the bent-core molecules was reproduced for the $\gamma = 40°$ bent-core model. Although not a common feature in the bent-core liquid crystal phase diagram, it highlights the importance of the bent-core shape in producing these phases.

ACKNOWLEDGMENTS

The authors would like to thank the Engineering and Physical Sciences Research Council which funded this work (GR/L76693). One of the authors, S.J., is grateful to the EPSRC for financial support. The authors would like to acknowledge useful conversations with Dr. Martin Grayson of Sheffield University.

[1] T. Niori, T. Sekine, J. Watanabe, T. Furukawe, and H. Takezoe, J. Mater. Chem. **6**, 1231 (1996).
[2] T. Sekine, T. Niori, J. Watanabe, T. Furukawe, S. Choi, and H. Takezoe, J. Mater. Chem. **7**, 1307 (1997).
[3] J. Matraszek, J. Mieczkowski, J. Szydlowska, and E. Gǿrecka, Liq. Cryst. **27**, 429 (2000).
[4] T. Sekine, T. Niori, J. Watanabe, T. Furukawa, S.W. Choi, and H. Takezoe, J. Mater. Chem. **7**, 1307 (1997).
[5] T. Niori, T. Sekine, J. Watanabe, T. Furukawa, and H. Takezoe, Mol. Cryst. Liq. Cryst. Sci. Technol., Sect. A **301**, 337 (1997).
[6] D.R. Link, G. Natale, R. Shao, J.E. Maclennan, N.A. Clark, E. Körblova, and D.M. Walba, Science **278**, 1924 (1997).
[7] S. Diele, S. Grande, H. Kruth, C.H. Lischka, G. Pelzl, W. Weissflog, and I. Wirth, Ferroelectrics **212**, 169 (1998).
[8] S.T. Lagerwall, J. Phys.: Condens. Matter **8**, 9143 (1996).
[9] H.R. Brand, P.E. Cladis, and H. Pleiner, Eur. Phys. J. B **6**, 347 (1998).
[10] D. Shen, S. Diele, I. Wirt, and C. Tschierske, Chem. Commun. (Cambridge) **8**, 2573 (1998).
[11] W. Weissflog, C.H. Lischka, I. Benné, T. Scharf, G. Pelzl, S. Diele, and H. Kruth, Proc. SPIE **3319**, 14 (1997).
[12] G. Pelzl, S. Diele, S. Grande, A. Jakli, C.H. Lischka, H. Kresse, H. Schmalfuss, I. Wirth, and W. Weissflog, Liq. Cryst. **26**, 401 (1999).
[13] M.P. Neal, A.J. Parker, and C.M. Care, Mol. Phys. **91**, 603 (1997).
[14] M.R. Wilson, and M.P. Allen, Mol. Cryst. Liq. Cryst. **198**, 465 (1991).
[15] M.A. Glaser, R. Malzbender, N.A. Clark, and D.M. Walba, J. Phys.: Condens. Matter **6**, 261 (1994).
[16] C. McBride, M.R. Wilson, and J.A.K. Howard, Mol. Phys. **93**, 955 (1998).
[17] D. Frenkel, H.N.W. Lerkkerkerer, and A. Stroobants, Nature (London) **332**, 822 (1988).
[18] P.I.C. Teixeira, A.J. Masters, and B.M. Mulder, Mol. Cryst. Liq. Cryst. Sci. Technol., Sect. A **323**, 167 (1998).
[19] J.G. Gay, and B.J. Berne, J. Chem. Phys. **74**, 3316 (1981).
[20] G.R. Luckhurst, R.A. Stephens, and R.W. Phippen, Liq. Cryst. **8**, 451 (1990).
[21] E. de Miguel, L.F. Rull, M.K. Chalam, and K.E. Gubbins, Mol. Phys. **74**, 405 (1991).
[22] L.F. Rull, Physica A **220**, 113 (1995).
[23] J.T. Brown, M.P. Allen, E.M. del Rio, and E. de Miguel, Phys. Rev. E **57**, 6685 (1998).
[24] R. Memmer, Liq. Cryst. **27**, 533 (2000).
[25] M.P. Neal, and A.J. Parker Chem. Phys. Lett. **294**, 277 (1998).
[26] P.J. Camp, M.P. Allen, and A.J. Masters, J. Chem. Phys. **111**, 9871 (1999).
[27] R. Memmer, and G. Schöbel (unpublished).
[28] J. Xu, R.L.B. Selinger, J.V. Selinger, and R. Shashidar, J. Chem. Phys. **115**, 4333 (2001).
[29] P.K. Maiti, Y. Lansac, M.A. Glaser, and N.A. Clark (unpublished).

[30] Y. Lansac, P.K. Maiti, M.A. Glaser, and N.A. Clark (unpublished).
[31] A. Derzhanski, and A.G. Petrov, Mol. Cryst. Liq. Cryst. **89**, 339 (1982).
[32] J. Stelzer, R. Berardi, and C. Zannoni, Chem. Phys. Lett. **299**, 9 (1999).
[33] R. Berardi, S. Orlandi, and C. Zannoni, Chem. Phys. Lett. **261**, 357 (1996).
[34] S.J. Johnston, R.J. Low, and M.P. Neal, Ferroelectrics (to be published).
[35] R. Berardi, A.P.J. Emerson, and C. Zannoni, J. Chem. Soc., Faraday Trans. **89**, 4069 (1993).
[36] D. Brown, and J.H.R. Clarke, Mol. Phys. **51**, 1243 (1984).
[37] S. Brode, and R. Aldrichs, Comput. Phys. Commun. **42**, 51 (1986).
[38] C. Zannoni, *The Molecular Physics of Liquid Crystals*, edited by G.R. Luckhurst, and G.W. Gray (Academic Press, New York, 1979).
[39] M.P. Allen, Liq. Cryst. **8**, 499 (1990).
[40] R. Hashim, G.R. Luckhurst, F. Prata, and S. Romano, Liq. Cryst. **15**, 283 (1993).
[41] W.H. Press, S.A. Teukolsky, W.T. Vetterling, and B.P. Flannery, *Numerical Recipes in Fortran, 2nd ed.* (Cambridge University Press, Cambridge, England, 1986).
[42] M.P. Neal, and A.J. Parker, Mol. Cryst. Liq. Cryst. Sci. Technol., Sect. A **330**, 565 (1999).
[43] J.P. Bedel, J.C. Rouillon, J.P. Marcerou, M. Laguerre, M.F. Achard, and H.T. Nguyen, Liq. Cryst. **27**, 103 (2000).
[44] S. Gupta, W.B. Seidewan, and E. Mclaughlin, Mol. Phys. **65**, 961 (1988).
[45] W.B. Seidewan, S. Gupta, and E. Mclaughlin, J. Chem. Phys. **90**, 1888 (1989).
[46] T. Sekine, T. Niori, M. Sone, J. Watanabe, S. Choi, Y. Takanashi, and H. Takezoe, Jpn. J. Appl. Phys., Part 1 **36**, 6455 (1997).